

Bloch-Zener Oscillations in Binary Superlattices

F. Dreisow,^{1,*} A. Szameit,¹ M. Heinrich,¹ T. Pertsch,¹ S. Nolte,¹ and A. Tünnermann^{1,2}

¹*Institute of Applied Physics, Friedrich-Schiller-University Jena, Max-Wien-Platz 1, 07743 Jena, Germany*

²*Fraunhofer Institute for Applied Optics and Precision Engineering, Albert-Einstein-Strasse 7, 07745 Jena, Germany*

S. Longhi

*Dipartimento di Fisica and Istituto di Fotonica e Nanotecnologie del CNR, Politecnico di Milano,
Piazza L. da Vinci 32, I-20133 Milano, Italy*

(Received 16 October 2008; revised manuscript received 12 January 2009; published 19 February 2009)

Bloch-Zener oscillations, i.e., the coherent superposition of Bloch oscillations and Zener tunneling between minibands of a binary lattice, are experimentally demonstrated for light waves in curved femtosecond laser-written waveguide arrays. Visualization of double-periodicity breathing and oscillation modes is reported, and synchronous tunneling leading to wave reconstruction is demonstrated.

DOI: 10.1103/PhysRevLett.102.076802

PACS numbers: 42.82.Et, 03.65.Xp, 73.21.Cd

Bloch oscillations (BOs) and Zener tunneling (ZT) are fundamental transport phenomena of electrons in periodic potentials [1]. In the absence of dephasing and scattering processes, an electron accelerated by an external dc electric field undergoes a coherent periodic motion (BO) which is related to the formation of a Wannier-Stark (WS) ladder energy spectrum. Tunneling to higher-order bands is responsible for BO damping and broadening of WS resonances. BOs and ZT have been impressively demonstrated in a number of experiments after the advent of semiconductor superlattices (see, e.g., [2]), and later on extended to various physical systems such as cold atoms and Bose-Einstein condensates in accelerating optical lattices [3], optical waves in photonic lattices [4–6], and acoustic waves in periodic media [7]. From the theoretical side, the interplay between BO and ZT has attracted much interest and different facets of the problem have been investigated (see, e.g., [8]). In multiband models, a cascade of ZT to higher-order bands usually occurs, and a rough estimate of BO damping is provided by the semiclassical Landau-Zener theory. The BO lifetime, however, does not decrease monotonically with field strength, but rather shows pronounced resonancelike drops (resonant ZT) whenever different WS ladders undergo avoided crossings [8]. The interplay between BOs and ZT in two-band models, such as that occurring in two minibands of a binary superlattice, shows an even richer scenario, including the possibility of Rabi-like oscillations, periodic reconstruction of an arbitrary initial wave packet, and complete arrest of ZT [9,10]. In physical space, a wave packet undergoes a characteristic double-period motion which is referred to as Bloch-Zener oscillation (BZO) [10,11]. BZOs have been theoretically investigated for both quantum particles [9,10] and classical waves [12], and their application to tunable matter wave beam splitters and Mach-Zehnder interferometry has recently been proposed [13]. Contrary to resonant ZT, which has been demonstrated recently in a few experiments for electrons [14], Bose-Einstein condensates [15]

and classical waves [6,7], observation of BZOs has not been reported yet to the best of our knowledge. In this Letter, we experimentally investigate ZT and BOs for light waves in a binary waveguide lattice and report on the observation of both synchronous and asynchronous BZOs in real space. As compared to other possible quantum or classical models of BOs and ZT phenomena, our waveguide-based superlattice enables a direct visualization of BZOs in physical space [16] and the possibility to excite either oscillation or breathing modes.

The paraxial propagation of linearly polarized optical waves at wavelength λ in a shallow one-dimensional lattice is governed by the Schrödinger-like equation

$$\left[i\lambda \frac{\partial}{\partial z} + \frac{\lambda^2}{2n_0} \frac{\partial^2}{\partial x^2} + \Delta n(x) \right] \psi = 0 \quad (1)$$

where $\lambda = \lambda/(2\pi)$ is the reduced wavelength; x and z are the transverse and longitudinal coordinates, respectively; $\Delta n(x)$ is the refractive index modulation; and n_0 is the refractive index of the bulk material. Equation (1) is analogous to the Schrödinger equation for a quantum particle in a periodic potential, provided that the spatial evolution along the longitudinal coordinate z is replaced by the temporal evolution of the particle wave function and the refractive index modulation $\Delta n(x)$ is replaced by the sign-reversed quantum mechanical potential $-V(x)$. In our system, $V(x)$ is a binary superlattice of period $2d$, composed by a sequence of alternating deep and shallow wells with equal spacing, which is superimposed to a linear gradient [Fig. 1(a)] realized by a circular bending (radius of curvature R) of the waveguides [17], as sketched in Fig. 1(d). In the waveguide reference frame, the curvature is perceived as an inertial (fictitious) constant force acting on light rays, which mimic the role of a dc field responsible for BOs and ZT. Because of the double-periodicity of the potential, the lowest band of the array splits into two minibands which are separated by a small gap [see Fig. 1(c)]. In the tight-binding limit, the dynamics are well described by the

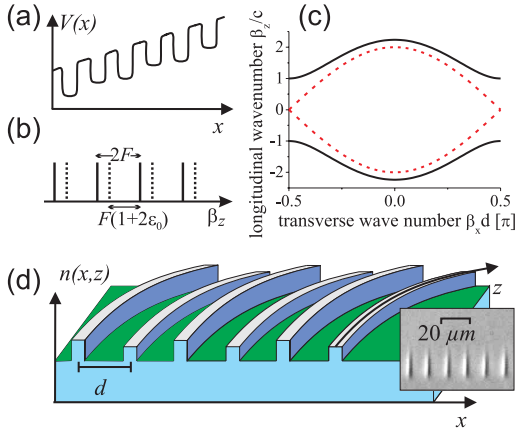


FIG. 1 (color online). Schematic sketch of the system: (a) transverse potential of a binary lattice with additional linear gradient; (b) interleaved WS ladder spectrum; (c) dispersion curves of tight-binding minibands with equal waveguides (dashed curve) and detuned ($\sigma = \kappa$) waveguides (solid curve); (d) two-dimensional refractive index profile of the circularly-curved waveguide array. The inset in (d) is a microscope image showing cross sections of a few waveguides realized in fused silica glass.

following set of coupled equations for the modal amplitudes a_m of light waves trapped in the various waveguides [10,18]

$$\left(i \frac{d}{dz} + (-1)^m \sigma + mF \right) a_m + \kappa (a_{m+1} + a_{m-1}) = 0, \quad (2)$$

where 2σ and κ are the propagation constant mismatch and the hopping rate between two adjacent waveguides of the array, respectively, and $F = n_0 d / R \lambda$ is the index gradient due to waveguide bending. For $F = 0$, i.e., for straight waveguides, inserting a plane wave ansatz $a_m \propto \exp[i(\beta_z z - m \beta_x d)]$ into Eqs. (2) yields the following dispersion relation for the two minibands [10,18]:

$$\beta_z^\pm = \pm \sqrt{\sigma^2 + 4\kappa^2 \cos^2 \beta_x d} \quad (3)$$

where β_z and β_x are the longitudinal and transverse propagation constants, respectively. Note that the two minibands are separated by a gap 2σ . When the waveguides are bent, the two minibands are replaced by two interleaved WS ladders, $\beta_{z,m}^{(1)} = (2m + \epsilon_0)F$ and $\beta_{z,m}^{(2)} = (2m + 1 - \epsilon_0)F$, where $m = 0, \pm 1, \pm 2, \dots$ and ϵ_0 determines the relative distance between the two WS ladders [see Fig. 1(b)]. The normalized offset ϵ_0 turns out to be a function of κ/F and σ/F solely and can be numerically computed from a spectral analysis of Eq. (2). The corresponding surface $\epsilon_0(\kappa/F, \sigma/F)$, depicted in Fig. 3 of Ref. [10], shows an oscillatory behavior between $-1/2$ and $1/2$, and vanishes over a sequence of curves in the $(\kappa/F, \delta/F)$ plane departing from the points $(0, \pm 1), (0, \pm 2), (0, \pm 3), \dots$

The waveguide arrays were realized by femtosecond laser microstructuring of 75-mm-long fused silica (Suprasil 311) samples [19]. To fabricate a binary array,

the writing velocities were lowered for every other waveguide, resulting in increased refractive index modulations and increased effective propagation constants of the respective guides [20].

In this special fused silica glass ($n_0 = 1.46$ in the visible), the femtosecond laser micromachining yields massive formation of color centers. Excited with a HeNe laser, these color centers emit fluorescence light and the propagation can be conveniently observed with a CCD camera by scanning the top of the sample (for details, see [21]). A coordinate transformation, from curvilinear to straight, is digitally applied to the images to obtain a better visualization of the beam dynamics.

The experiments were performed for two different lattice excitations, which enable to observe either breathing or oscillation modes [10]. In the first instance, breathing modes were observed by single waveguide excitation ($\lambda = 633$ nm) at the input plane. For $\sigma = 0$, the light broadens and refocuses again at multiples of the Bloch period $z_B = 2\pi/F = R\lambda/(n_0 d)$, showing a characteristic breathing pattern with the barycenter remaining on the input waveguide. This is shown in Fig. 2(a) for an array comprising two complete BO periods ($z_B = 37.5$ mm). In the reciprocal space, single site illumination corresponds to excitation of all Bloch modes of the two minibands with a flat Fourier spectrum. According to the acceleration theorem, the Bloch vectors drift through the reciprocal space, and tunneling between the minibands is complete at the band edge $\beta_x d = \pm \pi/2$, since here the minibands are in touch. Therefore, the band occupancies do not evolve along the

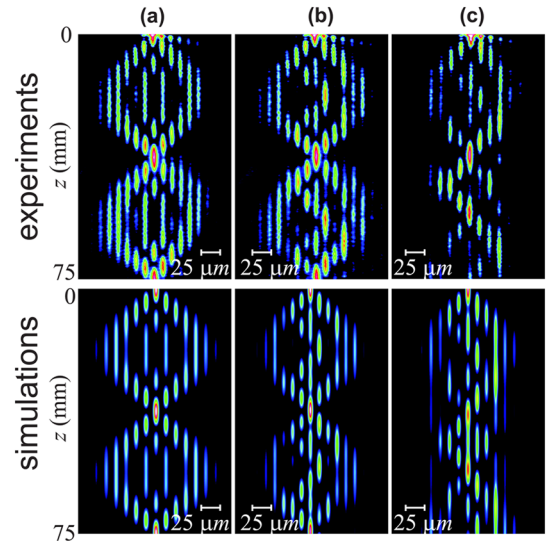


FIG. 2 (color online). Breathing modes in curved binary arrays for single waveguide excitation and for a Bloch period $z_B = 37.5$ mm. (a) $\kappa = 0.23$ mm $^{-1}$, no detuning; (b) $\kappa = 0.23$ mm $^{-1}$, $\sigma/\kappa = 0.4$, corresponding to synchronous ZT ($z_2 = z_B$); (c) $\kappa = 0.20$ mm $^{-1}$, $\sigma/\kappa = 0.4$, corresponding to asynchronous ZT. In (a) and (b), $d = 13$ μ m and $R = 1.12$ m; in (c), $d = 14$ μ m and $R = 1.21$ m. Upper figures: measured fluorescence images, lower figures: corresponding simulations.

propagation direction, and remain equal for the two minibands. As a gap between the two minibands is created ($\sigma \neq 0$), ZT at the band edges is not complete, and the breathing motion becomes generally aperiodic and can be characterized by two spatial periods [10]. The first one, z_1 , is determined by mode spacing of each WS ladder and equals half of the Bloch period, i.e., $z_1 = z_B/2$. The second one, which will be referred to as the Zener period, is determined by the shift of the two interleaved WS ladders and is given by $z_2 = 2\pi/|F(1 - 2\epsilon_0)|$ [see Fig. 1(b)]. If z_1 and z_2 are commensurate, ZT is synchronous with the BO motion, and perfect wave packet reconstruction is achieved [10]. In particular, if the waveguide spacing d , detuning σ , and radius of curvature R are tuned to get $\epsilon_0 \approx 0$, one has $z_2 = 2z_1 = z_B$ and wave packet reconstruction is observed after a full Bloch cycle. This is shown in Fig. 2(b), where the numerically computed value $\epsilon_0 \sim -0.019$ corresponds to a regime with $z_2 \approx 2z_1$. Conversely, in Fig. 2(c), the array parameters yield asynchronous ZT ($\epsilon_0 \sim 0.0905$), and wave reconstruction is not observed after one Bloch period.

The double periodicity involved in the breathing modes is best visualized in Fig. 3, which corresponds to arrays fabricated with a smaller waveguide spacing ($d = 11 \mu\text{m}$) and longer Bloch period ($z_B = 75 \text{ mm}$). While for the nondetuned array self-focusing occurs exclusively at z_B [Figs. 3(a)], the detuning of every other site yields a sub-periodicity with a period length of $z_1 = z_B/2$. Depending on the values of κ and σ , nearly synchronous [Figs. 3(b), corresponding to $\epsilon_0 \sim -0.01$] or asynchronous [Figs. 3(c), corresponding to $\epsilon_0 \sim -0.248$] BZO can be achieved.

To observe oscillation modes, in a second series of measurements, a set of three arrays were fabricated and excited with a broad Gaussian beam covering about 9

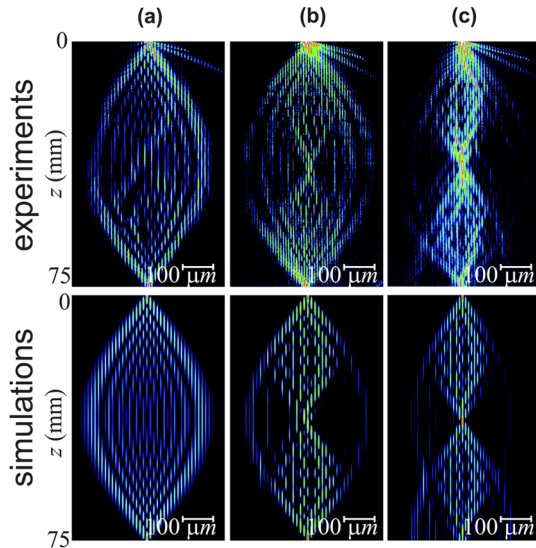


FIG. 3 (color online). Same as Fig. 2, but for $d = 11 \mu\text{m}$ and $R = 1.9 \text{ m}$, corresponding to $\kappa = 0.37 \text{ mm}^{-1}$ and $z_B = 75 \text{ mm}$. (a) no detuning; (b) $\sigma/\kappa = 0.3$ (synchronous ZT); (c) $\sigma/\kappa = 0.5$ (asynchronous ZT).

waveguides (FWHM) at the input plane. The geometric parameters of the arrays are $d = 11 \mu\text{m}$, $R = 1.90 \text{ m}$ (corresponding to $\kappa \approx 0.55 \text{ mm}^{-1}$ and $z_B = 75 \text{ mm}$); the writing velocities were set to achieve, for the three arrays, $\sigma = 0$, $\sigma \approx 0.22\kappa$, and $\sigma \approx 0.41\kappa$. For broad Gaussian excitation at normal incidence, a narrow spectrum of Bloch modes, centered around $\beta_x = 0$ and belonging to the first miniband, is excited at the input plane [18]. The linear potential accelerates the spectrum from $\beta_x = 0$ at $z = 0$ to $\beta_x = Fz/d$ at the generic plane z . Since ZT occurs when β_x is close to the band edges $\beta_x = \pm\pi/(2d)$, tunneling zones can be defined in spatial coordinate z around $z_{T1} = z_B/4$, $z_{T2} = 3z_B/4$, $z_{T3} = 5z_B/4, \dots$. For propagation distances z smaller than z_{T1} , the light beam is trapped mainly in the first miniband of the array and propagates along the direction locally orthogonal to the band dispersion curve. Around $z = z_{T1}$, a fraction of the beam tunnels into the second miniband. The strength of ZT is strongly dependent on the width and the gap of the band. Since the refraction angles of light waves in the two minibands have opposite signs [18], at $z = z_{T1}$, the beam breaks up into two parts, which follow different paths and refocuses at the second tunneling point $z = z_{T2}$. Here, the situation becomes more complex since both bands are occupied and the beams coherently interfere, yielding generally asynchronous tunneling (see Fig. 4). The beams belonging to the two different minibands are spatially separated since far from the crossing regions $z_{T1} = z_B/4$, $z_{T2} = 3z_B/4, \dots$ the fractional band occupancies can be simply estimated from the fluorescence images after inte-

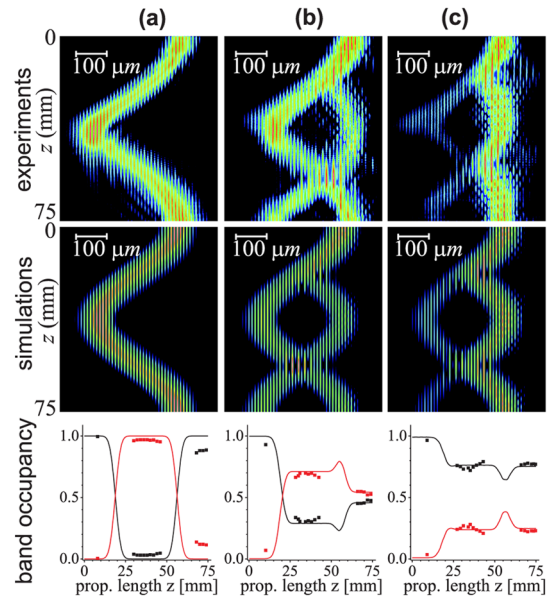


FIG. 4 (color online). Oscillation modes in binary waveguide arrays with $z_B = 75 \text{ mm}$. Measured fluorescence images and estimated fractional band occupancies, with corresponding theoretical predictions, for (a) $\kappa = 0.55 \text{ mm}^{-1}$ no detuning; (b) $\kappa = 0.55 \text{ mm}^{-1}$, $\sigma/\kappa = 0.22$; (c) $\kappa = 0.538 \text{ mm}^{-1}$, $\sigma/\kappa = 0.41$.

gration of the beam intensities over the transverse x direction. The fluorescence images and corresponding evolution of fractional band occupancies, measured in the three arrays for increasing values of σ/κ , are shown in Fig. 4 and compared to theoretical predictions based on the tight-binding model (2). For the first sample ($\sigma = 0$), pure BOs are observed [Fig. 4(a)], and tunneling between the minibands is complete as the gap between them vanishes. Detuned arrays with a gap between the two minibands show reduced ZT. For $\sigma = 0.22\kappa$ [Fig. 4(b)], the tunneling rate is $\approx 65\%$. With the chosen parameters, ZT is not synchronous ($\epsilon_0 \sim -0.155$) with BOs and light does not tunnel back completely into the first miniband after a full Bloch cycle [Fig. 4(b)], with approximately equal powers left in the two minibands. At a larger gap, ZT is weaker, and the initially excited band remains the most occupied one for the whole Bloch cycle [Fig. 4(c), $\epsilon_0 \sim -0.125$].

In conclusion, we experimentally investigated the interplay between BOs and ZT for light waves in optical binary superlattices. A direct visualization in physical space of synchronous and asynchronous ZT regimes, not explored in previous demonstrations of nonresonant or resonant ZT [5–7,15], has been reported. Besides their relevance as a basic dynamical phenomenon found for both classical waves and quantum particles in periodic systems [9,10,12], BZOs may offer potential applications for the realization of tunable beam splitters and interferometers for matter or light waves [13].

We acknowledge support by the Deutsche Forschungsgemeinschaft (Leibniz-Programm and R. U. 532 “Non-linear spatio-temporal dynamics in dissipative and discrete optical systems”).

*f.dreisow@uni-jena.de

- [1] F. Bloch, Z. Phys. **52**, 555 (1929); C. Zener, Proc. R. Soc. A **145**, 523 (1934).
- [2] P. Voisin, J. Bleuse, C. Bouche, S. Gaillard, C. Alibert, and A. Regreny, Phys. Rev. Lett. **61**, 1639 (1988); H. Schneider, H.T. Grahn, K.v. Klitzing, and K. Ploog, Phys. Rev. Lett. **65**, 2720 (1990); J. Feldmann, K. Leo, J. Shah, D.A.B. Miller, J.E. Cunningham, T. Meier, G. von Plessen, A. Schulze, P. Thomas, and S. Schmitt-Rink, Phys. Rev. B **46**, 7252 (1992); B. Rosam, D. Meinhold, F. Loser, V.G. Lyssenko, S. Glutsch, F. Bechstedt, F. Ross, K. Kohler, and K. Leo, Phys. Rev. Lett. **86**, 1307 (2001).
- [3] M. Ben Dahan, E. Peik, J. Reichel, Y. Castin, and C. Salomon, Phys. Rev. Lett. **76**, 4508 (1996); S.R. Wilkinson, C.F. Bharucha, K.W. Madison, Q. Niu, and M.G. Raizen, Phys. Rev. Lett. **76**, 4512 (1996); B.P. Anderson and M.A. Kasevich, Science **282**, 1686 (1998); O. Morsch, J.H. Muller, M. Cristiani, D. Ciampini, and E. Arimondo, Phys. Rev. Lett. **87**, 140402 (2001).
- [4] R. Morandotti, U. Peschel, J.S. Aitchison, H.S. Eisenberg, and Y. Silberberg, Phys. Rev. Lett. **83**, 4756 (1999); T. Pertsch, P. Dannberg, W. Elflein, A. Bräuer, and F. Lederer, Phys. Rev. Lett. **83**, 4752 (1999); R. Sapienza, P. Costantino, D. Wiersma, M. Ghulinyan, C. J. Oton, and L. Pavesi, Phys. Rev. Lett. **91**, 263902 (2003).
- [5] H. Trompeter, T. Pertsch, F. Lederer, D. Michaelis, U. Streppel, A. Bräuer, and U. Peschel, Phys. Rev. Lett. **96**, 023901 (2006); H. Trompeter, W. Krolikowski, D.N. Neshev, A.S. Desyatnikov, A.A. Sukhorukov, Yu.S. Kivshar, T. Pertsch, U. Peschel, and F. Lederer, Phys. Rev. Lett. **96**, 053903 (2006).
- [6] M. Ghulinyan, C.J. Oton, Z. Gaburro, L. Pavesi, C. Toninelli, and D.S. Wiersma, Phys. Rev. Lett. **94**, 127401 (2005).
- [7] H. Sanchis-Alepuz, Y.A. Kosevich, and J. Sánchez-Dehesa, Phys. Rev. Lett. **98**, 134301 (2007).
- [8] M. Glück, A.R. Kolovsky, and H.J. Korsch, Phys. Rep. **366**, 103 (2002).
- [9] J. Rotvig, A.-P. Jauho, and H. Smith, Phys. Rev. Lett. **74**, 1831 (1995); D.W. Hone and X.-G. Zhao, Phys. Rev. B **53**, 4834 (1996).
- [10] B.M. Breid, D. Witthaut, and H.J. Korsch, New J. Phys. **8**, 110 (2006).
- [11] BZOs should not be confused with “Rabi oscillations” observed when an ac field is introduced to resonantly induce transitions between Bloch states of different bands. Rabi oscillations between Bloch bands have been previously studied, e.g., in: X.-G. Zhao, G.A. Georgakis, and Q. Niu, Phys. Rev. B **54**, R5235 (1996); and experimentally observed for cold atoms in: M.C. Fischer, K.W. Madison, Q. Niu, and M.G. Raizen, Phys. Rev. A **58**, R2648 (1998).
- [12] S. Longhi, Europhys. Lett. **76**, 416 (2006).
- [13] B.M. Breid, D. Witthaut, and H.J. Korsch, New J. Phys. **9**, 62 (2007).
- [14] B. Rosam *et al.*, Phys. Rev. B **68**, 125301 (2003).
- [15] C. Sias, A. Zenesini, H. Lignier, S. Wimberger, D. Ciampini, O. Morsch, and E. Arimondo, Phys. Rev. Lett. **98**, 120403 (2007).
- [16] F. Dreisow, A. Szameit, M. Heinrich, T. Pertsch, S. Nolte, A. Tünnermann, and S. Longhi, Phys. Rev. Lett. **101**, 143602 (2008).
- [17] G. Lenz, I. Talanina, and C.M. de Sterke, Phys. Rev. Lett. **83**, 963 (1999); N. Chiodo, G. Della Valle, R. Osellame, S. Longhi, G. Cerullo, R. Ramponi, P. Laporta, and U. Morgner, Opt. Lett. **31**, 1651 (2006).
- [18] A.A. Sukhorukov and Y.S. Kivshar, Opt. Lett. **27**, 2112 (2002); R. Morandotti, D. Mandelik, Y. Silberberg, J.S. Aitchison, M. Sorel, D.N. Christodoulides, A.A. Sukhorukov, and Y.S. Kivshar, Opt. Lett. **29**, 2890 (2004).
- [19] K. Itoh, W. Watanabe, S. Nolte, and C.B. Schaffer, MRS Bull. **31**, 620 (2006).
- [20] D. Blomer, A. Szameit, F. Dreisow, T. Schreiber, S. Nolte, and A. Tünnermann, Opt. Express **14**, 2151 (2006).
- [21] A. Szameit, F. Dreisow, H. Hartung, S. Nolte, A. Tünnermann, and F. Lederer, Appl. Phys. Lett. **90**, 241113 (2007); F. Dreisow, M. Heinrich, A. Szameit, S. Döring, S. Nolte, A. Tünnermann, S. Fahr, and F. Lederer, Opt. Express **16**, 3474 (2008).